Theor Chim Acta (1993) 87: 5–17

Theoretica Chimica Acta

Theoretical rotational–vibrational spectra of the X^3B_1, a^1A_1 and b^1B_1 states of NH_2^+*

G. Chambaud[1,], W. Gabriel[1], T. Schmelz[1], P. Rosmus[1], A. Spielfiedel[2], and N. Feautrier[2]**

[1] Fachbereich Chemie der Universität D-60439 Frankfurt, Germany

[2] Observatoire de Paris, DAMAp, F-92195 Meudon, France

Received November 30, 1992/Accepted February 24, 1993

Summary. The three-dimensional potential energy functions have been calculated from highly correlated multireference configuration interaction electronic wavefunctions for the X^3B_1, a^1A_1, and b^1B_1 states of the NH_2^+ ion. For the quasi-linear electronic ground state this information and the electric dipole moment functions have been used to calculate spectroscopic constants, line intensities and rotationally resolved absorption spectra. For the a^1A_1–b^1B_1 bent/quasi-linear Renner–Teller system ro-vibronic energy levels have been obtained from a variational approach accounting for anharmonicity, rotation–vibration and electronic angular momenta coupling effects. The vibronic levels are given for energies up to 13 500 cm^{-1} for the bending levels and up to 8000 cm^{-1} for the stretching and combination levels.

Key words: Potential energy functions – NH_2^+ – Rotational–vibrational spectra

1 Introduction

Theoretical calculations predicted the NH_2^+ ion to be quasi-linear with a very low potential barrier at linearity [1, 2]. To date, the geometric structure and an unequivocal experimental evidence of the quasi-linearity has not been known. The only high resolution study of NH_2^+ has been published by Okumura, Rehfuss, Dinelli, Bawendi, and Oka [3], who investigated the ν_3 band in direct absorption using a tunable difference frequency laser spectrometer. The band origin was found to be $\nu_3 = 3359.932\ cm^{-1}$. Very recently, four new hot bands involving the excitation of ν_1 and/or ν_2 have been recorded and assigned by Huet, Kabbadj, Gabrys, and Oka [4]. Dunlavey, Dyke, Jonathan, and Morris [5] observed the photoelectron spectrum of the NH_2 radical and found for the ion $\nu_2 = 840 \pm 50\ cm^{-1}$. Herzberg [6] detected emission lines from ammonia ionized by collisions with low energy electrons, which he tentatively assigned to the NH_2^+ spectrum.

* Dedicated in the honor of Prof. Werner Kutzelnigg

** *Permanent address*: Université de Marne la Vallée, Départment Matériaux, F-93160 Noisy le Grand, France

As in the case of isoelectronic CH_2, the first two low-lying singlet states, a^1A_1 and b^1B_1 become a degenerate $^1\Delta_g$ state at linearity and, therefore, both electronic states are coupled by the Renner–Teller effect. For CH_2 more than 10000 transitions within these first two Renner–Teller singlet states have been measured [7] and partly assigned, but no such transitions have yet been detected for NH_2^+.

There have been several *ab initio* studies of NH_2^+. Peyerimhoff und Buenker [2] calculated many properties of the lowest fourteen electronic states of NH_2^+. Later, Peric, Buenker, and Peyerimhoff [8] dealt with the electron-nuclear motion coupling problem in the first electronically excited $^1A_1$ and $^1B_1$ states. They employed the theoretical MRD-CI potential energy functions in a variational method which took into account the Renner–Teller coupling and the large amplitude bending motion in an effective one-dimensional Hamiltonian. DeFrees and McLean [9] calculated vibrational harmonic frequencies of NH_2^+ in its ground state. So far, the most accurate theoretical study of the spectroscopic data for NH_2^+ has been published by Jensen, Bunker, and McLean [1]. They calculated the potential energy functions (PEFs) of the three lowest electronic states and obtained rotation–vibration energies for two of these states. The Renner–Teller coupling in the singlet states has been neglected.

For CH_2, extensive calculations have been made and it has become the benchmark triatomic species for testing *ab initio* quantum chemistry methods (for the Renner–Teller problem in CH_2 and review of the previous works cf. Ref. [10]). Similarly, the isoelectronic NH_2^+ ion, with its six valence electrons, represents an electronic problem small enough to be treated with high precision. In the present work such extensive electronic structure calculations have been employed to obtain three-dimensional potential energy and electric dipole moment functions, spectroscopic constants, absolute line intensities and rotationally resolved spectra.

2 Electronic structure calculation

In the electronic structure calculations we have used two different basis sets. The larger basis set $[B_1]$ consisted of the correlation consistent (14*s*8*p*4*d*3*f*2*g*) basis set of Dunning [11] contracted to [6*s*5*p*4*d*3*f*2*g*] according to the general contraction scheme for N and of the corresponding (6*s*3*p*2*d*1*f*) basis set for H contracted to [4*s*3*p*2*d*1*f*]. The total number of contracted Gaussian functions was 140. The second basis set $[B_2]$ consisted of the (12*s*6*p*3*d*2*f*) [11] contracted to [5*s*4*p*3*d*2*f*] according to the general contraction scheme for N and of the corresponding (6*s*3*p*2*d*) basis set for H contracted to [4*s*3*p*2*d*]. In this case the total number of contracted Gaussian functions was 92.

The near-equilibrium PEFs for the X^3B_1, a^1A_1, and b^1B_1 states were mapped for 150 geometries with both basis sets for bond lengths 1.55 bohr $< R_{NH} <$ 3.00 bohr and included angle $75° < \alpha < 180°$ by a multireference internally contracted configuration interaction (MRCI) [12–15] approach using the MOLPRO code [16]. The reference wavefunctions and the correlation orbitals were obtained from complete active space self-consistent field (CASSCF) calculations with active space comprising all valence orbitals; the core (1*s* of N) orbital was kept doubly occupied in all configurations. At the CASSCF level the X^3B_1 (A'') state has been calculated alone and the $^1A_1$ (A') and $^1B_1$ (A'') states were optimized together in a state-averaged procedure; each component having the same weight. For structures in C_s symmetries this resulted in 99 CSF's for the $^3A''$ state, 100 CSF's for the $^1A'$ and 75 CSF's for the $^1A''$ states. The reference wavefunctions in the MRCI calculations

comprised all the configurations of the CASSCF calculation. The core electrons were not correlated. The electric dipole moments were calculated as expectation values.

3 Potential energy and dipole moment functions

The calculated total MRCI energies of the three electronic states for 150 near-equilibrium geometries were fitted by polynomial functions:

$$V(R_1, R_2, \alpha) = \Sigma_{ijk}\, C_{ijk}\, (q_1)^i (q_2)^j (q_3)^k,$$

in the bond lengths R_1, R_2 and the included bond angle α. The coordinates q_1 and q_2 were Simon–Parr–Finlan coordinates of the form $q_i = 1 - R^{ref}/R_i$. For q_3 the displacement coordinate $(\alpha - \alpha^{ref})$ was used. In our fits of the three PEF's the root mean squares were less than 2 cm^{-1}. Only the expansion coefficients of the PEF's obtained with a large basis set $[B_1]$ are given in Table 1, the results calculated with

Table 1. Expansion coefficients of the three-dimensional near equilibrium PEFs of the three lowest electronic states of NH_2^+ (in a.u.)

X^3B_1 state[a]							
C_{000}:	−55.4346987	C_{100}:	0.0067603	C_{001}:	0.0007056	C_{200}:	0.7694751
C_{110}:	−0.0240565	C_{101}:	0.0051808	C_{002}:	0.0163100	C_{300}:	−0.1674700
C_{210}:	−0.0131014	C_{201}:	−0.0029595	C_{111}:	−0.0097988	C_{102}:	−0.0090767
C_{003}:	−0.0297731	C_{400}:	−0.3035577	C_{310}:	−0.0163155	C_{220}:	−0.0580796
C_{301}:	−0.0201707	C_{211}:	−0.0053209	C_{202}:	−0.0208717	C_{112}:	0.0374995
C_{103}:	0.0087475	C_{004}:	0.0033145	C_{500}:	−0.1219646	C_{410}:	0.0230236
C_{320}:	−0.0803918	C_{401}:	−0.0586619	C_{311}:	0.0848294	C_{221}:	−0.0549291
C_{302}:	0.0114040	C_{212}:	−0.0098973	C_{203}:	0.0188437	C_{113}:	−0.0064798
C_{104}:	−0.0043093	C_{005}:	0.0068723	C_{600}:	0.0691383	C_{510}:	0.3176133
C_{420}:	0.1722048	C_{330}:	−0.5094763	C_{501}:	−0.0980143	C_{411}:	0.3042142
C_{321}:	−0.1283185	C_{402}:	0.0621450	C_{312}:	−0.0440334	C_{222}:	−0.0394200
C_{303}:	0.0240131	C_{213}:	0.0036048	C_{204}:	0.0471765	C_{114}:	−0.0920737
C_{105}:	−0.0023306	C_{006}:	0.0024627				
a^1A_1 state[b]							
C_{000}:	−55.3882786	C_{100}:	0.0001106	C_{001}:	0.0000047	C_{200}:	0.7337182
C_{110}:	−0.0057245	C_{101}:	0.0414585	C_{002}:	0.0665835	C_{300}:	−0.1659903
C_{210}:	−0.0029749	C_{201}:	0.0260878	C_{111}:	−0.0796721	C_{102}:	−0.0339958
C_{003}:	−0.0310118	C_{400}:	−0.3482419	C_{310}:	−0.1494518	C_{220}:	0.2644391
C_{301}:	−0.0538683	C_{211}:	−0.0039857	C_{202}:	−0.0327394	C_{112}:	0.1128163
C_{103}:	0.0263036	C_{004}:	−0.0158865	C_{500}:	−0.0899358	C_{410}:	−1.0367294
C_{320}:	0.8559873	C_{401}:	−0.2061575	C_{311}:	0.3903738	C_{221}:	−0.3783757
C_{302}:	0.0863695	C_{212}:	0.1512236	C_{203}:	0.0136437	C_{113}:	−0.0387548
C_{104}:	−0.0052160	C_{005}:	−0.0055623	C_{600}:	0.0859523	C_{510}:	−1.8198532
C_{420}:	0.0607169	C_{330}:	2.9002743	C_{501}:	−0.1266676	C_{411}:	1.0703439
C_{321}:	−1.1570981	C_{402}:	0.2129615	C_{312}:	−0.0930154	C_{222}:	−0.0577043
C_{303}:	−0.0471381	C_{213}:	−0.1258768	C_{204}:	0.0027785	C_{114}:	−0.0120508
C_{105}:	−0.0031308	C_{006}:	0.0094902				

Table 1. Continued

b^1B_1 state[c]

C_{000}: − 55.3651853	C_{100}: − 0.0004760	C_{001}: − 0.0000105	C_{200}: 0.7793620
C_{110}: − 0.0291541	C_{101}: 0.0154255	C_{002}: 0.0094927	C_{300}: − 0.1620015
C_{210}: − 0.0291878	C_{201}: 0.0092842	C_{111}: − 0.0152450	C_{102}: − 0.0181644
C_{003}: − 0.0254124	C_{400}: − 0.2821623	C_{310}: − 0.0239262	C_{220}: − 0.0493115
C_{301}: 0.0109633	C_{211}: − 0.0027823	C_{202}: − 0.0135164	C_{112}: 0.0295109
C_{103}: 0.0021417	C_{004}: 0.0118681	C_{500}: − 0.1923648	C_{410}: 0.0139861
C_{320}: − 0.0114226	C_{401}: 0.2527436	C_{311}: 0.0183335	C_{221}: − 0.0155254
C_{302}: − 0.2015783	C_{212}: 0.0909478	C_{203}: 0.0595742	C_{113}: 0.0148099
C_{104}: − 0.0021929	C_{005}: 0.0096695	C_{600}: − 0.0650453	C_{420}: − 0.0131727
C_{330}: − 0.0129058	C_{411}: − 0.0176073	C_{321}: − 0.0340287	C_{402}: 0.2150029
C_{312}: 0.0086526	C_{222}: − 0.0022866	C_{303}: − 0.3506929	C_{213}: − 0.0120271
C_{204}: 0.0227676	C_{114}: 0.0370737	C_{006}: − 0.0005906	C_{700}: − 0.0226973
C_{430}: − 0.0037089	C_{421}: − 0.0024083	C_{331}: − 0.0058637	C_{412}: 0.0231982
C_{322}: 0.0069713	C_{403}: 0.0736598	C_{313}: − 0.0041157	C_{223}: − 0.0186062
C_{304}: − 0.2397960	C_{214}: − 0.0070567	C_{007}: − 0.0018762	

[a] $R_1^{ref} = R_2^{ref} = 1.9538$ bohr, $\alpha^{ref} = 153.170°$, $C_{ijk} = C_{jik}$.
[b] $R_1^{ref} = R_2^{ref} = 1.9774$ bohr, $\alpha^{ref} = 108.386°$, $C_{ijk} = C_{jik}$.
[c] $R_1^{ref} = R_2^{ref} = 1.9440$ bohr, $\alpha^{ref} = 160.920°$, $C_{ijk} = C_{jik}$.

Table 2. Expansion coefficients of the three-dimensional near equilibrium dipole moment functions of the X^3B_1 electronic ground state[a] of NH_2^+ (in a.u.)

z-component[b]

C_{000}: .00000	C_{100}: .51869	C_{200}: .12913	C_{101}: .20812
C_{300}: − .02509	C_{210}: − .01409	C_{201}: .03991	C_{102}: − .13179
C_{400}: − .01827	C_{310}: − .00033	C_{301}: − .01662	C_{211}: .01426
C_{202}: − .02774	C_{103}: − .10859		

x-component[c]

C_{000}: .26687	C_{100}: .12019	C_{001}: − .49812	C_{200}: .03126
C_{110}: − .03386	C_{101}: − .23887	C_{002}: − .11475	C_{300}: − .00487
C_{210}: − .01138	C_{201}: − .06642	C_{111}: .07249	C_{102}: − .02238
C_{003}: .01554	C_{400}: − .00084	C_{310}: .00027	C_{220}: − .00124
C_{301}: .00927	C_{211}: .02345	C_{202}: .00897	C_{112}: − .00766
C_{103}: .01386	C_{004}: .02065		

[a] $R_1^{ref} = R_2^{ref} = 1.9453$ bohr, $\alpha^{ref} = 152.074°$.
[b] $C_{ijk} = -C_{jik}$.
[c] $C_{ijk} = C_{jik}$.

a smaller basis set $[B_2]$ will be discussed in the next section. These analytic functions define the PEFs of NH_2^+ in the geometry range of about $1.55 < R_{NH} < 2.55$ bohr and $80° < \alpha < 180°$. The dipole moment values have been transformed to the center of mass and fitted to similar polynomial expansions as the PEFs. In this case all three coordinates were the displacement coordinates

$(R_i - R^{ref})$ or $(\alpha - \alpha^{ref})$. The expansion coefficients of these functions are given in Table 2.

One-dimensional cuts of the MRCI PEFs along the bending coordinate are displayed in Fig. 1. It shows that the triplet ground state and the second singlet state have only very small barriers to linearity, smaller than in the isoelectronic CH_2 [10]. The two singlet states correlate with a $^1\Delta_g$ state at linearity, i.e. the nuclear and electron motion can not be treated separately, both states are coupled by the Renner–Teller effect.

In linear structures the $^1\Delta$ state crosses with the $^1\Pi$ state since the $^1\Delta$ state correlates diabatically with the $NH(^1\Delta) + H^+$ asymptote, whereas the $NH^+(^2\Pi) + H$ asymptote – which lies energetically lower – correlates with the $^1\Pi$ states. In additional calculations it was found that the crossing of both states in linear geometries occurs for fixed $R_1 = 1.9538$ bohr at about $R_2 = 4.25$ bohr and around 37 000 cm^{-1} above the minimum energy of the a^1A_1 state. Peyerimhoff and Buenker [2] found another conical intersection resulting from the crossing of the $^1A_2$ and b^1B_1 states for angles close to 70 degrees and $R_1 = R_2 = 1.9407$ bohr. This crossing occurs around 35 000 cm^{-1} above the minimum of the a^1A_1 state. Both regions of the conical intersections on the PEFs of the lowest two singlet states will, therefore, not influence the vibronic states lying below 15 000 cm^{-1}, which are of interest in the present work.

4 Ro-vibrational spectrum of the electronic ground state X^3B_1

Variational calculations for the rotational–vibrational levels of the quasi-linear electronic ground state were performed with the MRCI PEFs using the procedure of Carter and Handy [17] for $J = 0$ to 8. The basis set comprised 18 one-dimensional harmonic oscillator eigenfunctions for the stretching and 40 associated Legendre functions for the bending modes. Some of the resulting vibrational transition energies and the spectroscopic constants are compared with available experimental data and previous theoretical values in Table 3. The equilibrium structure (basis set $[B_1]$) has been calculated to be 1.0294 Å and 152.07°. The augmentation of the one-particle basis set (basis set $[B_1]$ vs. $[B_2]$, cf. Table 3) hardly influenced the equilibrium geometry, but changed the shape of the PEF, particularly along the stretching coordinates. The experimental ν_3 band origin of 3359.932 cm^{-1} [3] lies between our values calculated with the basis sets $[B_1]$ (3368.7 cm^{-1}) and $[B_2]$ (3353.4 cm^{-1}). Similarly, the energy differences calculated for the hot bands with the large basis set $[B_1]$ are all higher by about 8 to 10 cm^{-1} than the experimental values. Our equilibrium distance is slightly shorter and the equilibrium angle smaller than the values calculated by Jensen et al. [1] (cf. Table 3). The barrier to linearity of 260 cm^{-1} is larger by 51 cm^{-1} than their value. Jensen et al. [1] have empirically adjusted the values for the fundamental vibrational transitions for $\nu_1 = 3118\ cm^{-1}$, $\nu_2 = 918\ cm^{-1}$, and $\nu_3 = 3363\ cm^{-1}$, respectively. Our stretching wavenumbers are somewhat larger and the bending wavenumber lower than these values. Their calculated values are given in Table 3.

In Table 4 we have compared some rotation-bending levels calculated by Jensen et al. [1] with the values obtained with the PEF given in Table 1. Our, probably more precise values, are lower due to the flatter PEF along the bending coordinate. The pattern of the bending levels up to 10 000 cm^{-1} with different

Table 3. Spectroscopic parameters of the X^3B_1 electronic ground state of NH_2^+

X^3B_1	This work $[B_1]^a$	This work $[B_2]^a$	Ref. [1]	Ref. [4]
R_e (Å)	1.029	1.030	1.0338	
α_e(°)	152.07	151.76	153.17	
10^00–00^00(cm^{-1})[b]	3128.4	3116.8	3102	
02^00–00^00(cm^{-1})	913.7	909.3	922	
00^01–00^00(cm^{-1})	3368.7	3354.7	3344	3359.934[c]
10^01–10^00(cm^{-1})	3234.8	3222.1		3226.037
20^01–20^00(cm^{-1})	3091.0	3080.3		3081.548
01^11–01^10(cm^{-1})	3354.9	3340.4		3344.928
11^11–11^10(cm^{-1})	3221.4	3207.5		3211.341
02^01–02^00(cm^{-1})	3341.8	3326.9		3331.150
Rotational constants				
A_e (cm^{-1})	155.08	152.71		
B_e (cm^{-1})	8.38	8.37		
C_e (cm^{-1})	7.95	7.93		
Barrier to linearity (cm^{-1})	260	270	209	

[a] MRCI results calculated with the basis sets $[B_1]$ and $[B_2]$, cf. text.
[b] the theoretical transition energies are the energy differences between the corresponding lowest $K_a = 0$ or $K_a = 1$ levels in the bent notation (cf. Table 5).
[c] vibrational band origins from the fits to the observed transitions

Table 4. Comparison of rotational–vibrational levels in the electronic ground state X^3B_1 of NH_2^+, NHD^+, and ND_2^+ (in cm^{-1})

$v_2^{l\,a}$	v_2^b	K_a	N	NH_2^+ This work	Ref. [1]	NHD^+ This work	Ref. [1]	ND_2^+ This work	Ref. [1]
0^0	0	0	0	0.00	0.00	0.00	0.00	0.00	0.00
		0	1	15.95	15.80	10.87	10.76	8.03	7.95
		0	2	47.86	47.40	32.60	32.28	24.09	23.84
1^1		1	1	319.12	328.44	256.60	266.38	189.50	199.41
		1	2	350.78	359.80	278.21	287.79	205.49	215.24
2^2		2	2	759.90	775.45	621.08	637.35	468.68	485.18
3^3		3	3	1283.83	1302.94	1059.62	1079.89	808.64	829.54
4^4		4	4	1872.55	1893.46	1556.07	1578.71	1195.69	1219.56
2^0	1	0	0	913.66	922.45	764.41	772.11	602.57	608.29
		0	1	929.81	938.49	775.38	783.01	610.68	616.33
		0	2	962.10	970.56	797.35	804.20	626.89	632.42
3^1		1	1	1473.91	1481.55	1231.23	1240.03	966.47	975.79
		1	2	1505.52	1512.88	1252.84	1261.45	982.47	991.65
4^2		2	2	2074.39	2085.40	1734.57	1747.54	1360.60	1374.87
4^0	2	0	0	2146.75	2161.93	1801.81	1816.83	1424.38	1438.12
		0	1	2163.09	2178.17	1812.91	1827.85	1432.59	1446.27
		0	2	2195.79	2210.67	1835.12	1849.91	1449.00	1462.57

[a] linear notation
[b] bent notation

K_a values is displayed in Fig. 2. For $K_a = 0$ one clearly recognizes the inverse anharmonicity in the bending levels, the energy differences increase with increasing bending quanta. The quasi-linearity leads to the inversion of some levels relative to their positions in linear molecules. For example, in bent notation, the $v_2 = 1$, $K_a = 0$ level lies in NH_2^+ above the $v_2 = 0$, $K_a = 2$ level, etc. (cf. Fig. 2).

In Table 5 additional vibrational levels for energies up to about 7000 cm^{-1} and up to $K_a = 3$ are given. Since the NH_2^+ ion has been produced in various excited vibrational levels, such data could prove useful in the search for additional transitions needed for a better characterization of the quasi-linear nature of the electronic ground state.

The three-dimensional nuclear motion eigenfunctions have been used together with the *ab initio* calculated electric dipole moment functions in the evaluation of absolute line intensities for transitions up to $J = 8$ (cf. Ref. [18] for details of the method used in the calculations). The splittings due to the electron spin have been neglected, but the nuclear spin statistical weights have been considered. In Table 6 the most intense lines within the *P*-, *Q*- and *R*-branches for the fundamental absorption transitions at 300 K are given and the rotationally resolved spectra for transitions up to $J' = 8$ are displayed in Figs. 3 to 6. Even though the PEF is not accurate enough to describe the rotational – vibrational coupling very precisely (vibrational term values are accurate to within about 10 cm^{-1}), the following holds. The *P*- and *R*-transitions of the antisymmetric stretching mode are more intense by far than those of the symmetric stretching and bending modes. This could explain why only the antisymmetric stretching mode, and not the bending mode or the symmetric stretching mode, has been detected experimentally, even though both

Table 5. Calculated rotational–vibrational levels for low-lying states in the electronic ground state of NH_2^+ (in cm^{-1})

State	$K_a = 0$	State	$K_a = 1$	State	$K_a = 2$	State	$K_a = 3$
(0 0 0)	0.0	(0 0 0)	319.1	(0 0 0)	759.9	(0 0 0)	1283.8
(0 1 0)	913.7	(0 1 0)	1473.9	(0 1 0)	2074.4	(0 1 0)	2717.5
(0 2 0)	2146.7	(0 2 0)	2831.5	(0 2 0)	3535.9	(0 2 0)	4263.7
(1 0 0)	3128.4	(1 0 0)	3447.5	(1 0 0)	3885.9	(1 0 0)	4406.9
(0 0 1)	3368.7	(0 0 1)	3674.0	(0 0 1)	4100.0	(0 0 1)	4608.5
(0 3 0)	3576.2	(0 3 0)	4337.4	(0 3 0)	5106.1	(1 1 0)	5811.5
(1 1 0)	4034.9	(1 1 0)	4592.1	(1 1 0)	5194.8	(0 3 0)	5918.8
(0 1 1)	4255.5	(0 1 1)	4799.7	(0 1 1)	5384.4	(0 1 1)	6011.6
(0 4 0)	5131.8	(1 2 0)	5906.1	(1 2 0)	6618.4	(1 2 0)	7338.8
(1 2 0)	5262.8	(0 4 0)	5984.2	(0 4 0)	6797.4	(2 0 0)	7451.7
(0 2 1)	5457.5	(0 2 1)	6126.4	(0 2 1)	6814.8	(0 2 1)	7524.9
(2 0 0)	6178.9	(2 0 0)	6497.5	(2 0 0)	6933.3	(1 0 1)	7601.9
(1 0 1)	6363.2	(1 0 1)	6668.9	(1 0 1)	7093.7	(0 4 0)	7635.3
(1 3 0)	6654.3	(0 0 2)	6958.8	(0 0 2)	7371.8	(0 0 2)	7866.5
(0 0 2)	6665.1	(1 3 0)	7408.2	(1 3 0)	8157.0	(2 1 0)	8832.2
(0 5 0)	6813.7	(0 3 1)	7600.6	(2 1 0)	8240.8	(1 1 1)	8978.2
(0 3 1)	6855.7	(2 1 0)	7630.5	(1 1 1)	8335.4	(1 3 0)	8979.5
(2 1 0)	7077.7	(0 5 0)	7672.2	(0 3 1)	8392.3	(0 3 1)	9148.2
(1 1 1)	7243.7	(1 1 1)	7786.3	(0 5 0)	8539.5	(0 1 2)	9240.8

Table 6. Absolute absorption line intensities[a] (in bent notation) for the most intense lines of the fundamental transitions in the X^3B_1 electronic ground state of NH_2^+

	J'	K'_a		J''	K''_a	ΔE [cm^{-1}]	Line intensity [$atm^{-1}\,cm^{-2}$ at 300 K]	R^2 [in a.u.^{2}]
vibrational band 100–000								
P	3	1	–	4	0	3365.8	4.5	0.6364 – 1
Q	4	1	–	4	0	3433.9	5.5	0.1525 + 0
R	5	1	–	4	0	3505.8	10.4	0.9178 – 1
vibrational band 010–000								
P	2	0	–	3	0	563.8	12.4	0.4330 – 1
Q	4	0	–	4	0	608.4	23.2	0.1593 – 1
R	6	0	–	5	0	712.2	11.8	0.5762 – 1
vibrational band 001–000								
P	3	0	–	4	0	3302.8	166.5	0.1160 – 2
Q	1	1	–	1	1	3355.5	28.9	0.1367 – 2
R	5	0	–	4	0	3443.1	231.0	0.2538 – 2

[a] From the dipole transition matrix elements R^2 (in a.u.^{2}; since it is calculated from the ro-vibrational wavefunctions exactly, they include already the Honl-London and the $2J + 1$ degeneracy factors), the individual line intensities were calculated (cf. Ref. [18]) from the formula:

$$S_i = 3054.6\, g_{NS} \nu_i R^2 \exp(-E_r/kT)\,[1 - \exp(-\nu_i/kT]/(TQ_r)$$

where S_i is in $cm^{-2}\,atm^{-1}$, T is the temperature in K, g_{NS} is the nuclear spin statistical weight (1 or 3), ν_i is the transition frequency in cm^{-1}, R^2 is the squared dipole transition matrix element in D^2 (including already the degeneracy factor), E_r is the energy of the rotational levels in cm^{-1}, k is the Boltzmann constant, and Q_r the purely rotational partition function, which has been calculated from the formula $Q_r = \Sigma\, g_{NS}(2J + 1)\exp(-E_r/kT)$ for 300 K and $J \leq 10$ to be 79.

stretching modes overlap strongly in the experimentally investigated region between 3500 and 2900 cm^{-1}. Moreover, the symmetric stretching mode shows strong intensity anomalies due to the strong rotational–vibrational coupling. For this reason, as in H_2S [19], the P-branch has been calculated to be distinctly less intense than the R-branch. Also the fact that no transition from $K_a = 2$ has been observed is – at least partly – due to very small transition probabilities, which were calculated to be 5 to 10 times weaker than those from $K_a = 1$ levels for the ν_3 band.

5 Ro-vibronic spectrum of the a^1A_1 and b^1B_1 states

In Table 7 the spectroscopic constants for the a^1A_1 and b^1B_1 states obtained from the MRCI PEFs are given and compared with previous calculations. The a^1A_1 state is strongly bent, whereas the b^1B_1 state is quasi-linear. The barrier to linearity for the lower state has been calculated to be 5132 cm^{-1}, and for the upper state to be only 62 cm^{-1}. The equilibrium geometries, barriers to linearity and the excitation energies – apart from the bond angle of the upper state – agree well with the

Table 8. Bending levels ($J = K_a$) for the a^1A_1 and b^1B_1 states of NH_2^+ (in cm^{-1})

a^1A_1			b^1B_1		
v_2^{bent}	$K_a = 0$	$K_a = 1^a$	v_2^{lin}	$K_a = 0$	$K_a = 1^a$
0	0	33	0	5688	
1	1327	1363	1		6208
2	2593	2629	2	7093	
3	3789	3812	3		7649
4	4921	4838	4	8642	
5	6031	5595	5		9458
6	7179	6677	6	10310	
7	8395	7956	7		11158
8	9677	9008	8	12052	
9	11018	10345	9		12916
10	12398[b]	11722[b]	10	13860	
11	14038[c]	13121[c]	11		

[a] The mean value of the two K_c components is given
[b] Fermi resonance with (1 8 0) level
[c] Fermi resonance with (1 9 0) level

most accurate values so far of Jenssen et al. [1] (cf. Table 7). Our fundamental frequencies for the lower state are, however, generally higher by 20 to 40 cm^{-1}. The singlet–triplet separation $^{1,3}T_e$ has been calculated to be 10 193 cm^{-1}. The MRCI vertical excitation energy from the a^1A_1 state (at its equilibrium geometry) to the b^1B_1 state, amounts to 11 841 cm^{-1}.

The PEFs given in Table 1 were used in three-dimensional Renner–Teller variational calculations [20], in which the full dimensionality, anharmonicity, rotational–vibrational, and electronic angular momentum coupling effects have been taken into account. The basis set comprised 18 one-dimensional harmonic oscillator eigenfunctions for the stretching and 40 associated Legendre functions for the bending modes. Approximations were made for the electron angular momentum operators. The matrix elements $\langle a|L_z|b\rangle$, $\langle a|L_z^2|a\rangle$ and $\langle b|L_z^2|b\rangle$ were set to their values for a linear Δ state, i.e. their geometry dependence has not been considered. All other angular momentum matrix elements were omitted. The ro-vibronic spectrum has been evaluated for the energy region up to about 13 500 cm^{-1} above the minimum energy of the a^1A_1 state. The bending levels for $K_a = 0$ (Σ states) and 1 (Π states) are given in Table 8. In a singlet electronic state the Σ levels can be fully associated with one or the other PEF, whereas for the Π states the Born–Oppenheimer approximation is no more valid. Such a vibronic bending level exhibits strong electron-nuclear motion coupling. On the other hand, the levels with excited stretching modes can – to a large extent – be associated with only one PEF. Hence, in the AH_2 Renner–Teller systems relatively few vibronic levels (bending above the barrier, $K_a > 0$) are embedded in a manifold of vibrational levels for which the Born–Oppenheimer approximation holds relatively well. On the whole, up to 13 500 cm^{-1}, there are 46 symmetric (vibrational symmetry only), 28 antisymmetric, in the upper electronic states 12 symmetric and 6 antisymmetric Σ levels in NH_2^+. The bending levels of the lower singlet state exhibit normal

Table 7. Spectroscopic parameters of the a^1A_1 and b^1B_1 states of NH_2^+

a^1A_1	This work		Ref. [1]	Ref. [8]
	$[B_1]^a$	$[B_2]^a$		
R_e(Å)	1.046	1.047	1.051	
α_e(°)	108.38	108.07	108.37	
ν_1	3050	3033	3027	
ν_2	1327	1332	1289	
ν_3	3133	3120	3111	
Rotational constants				
A_e(cm^{-1})	25.53	25.27		
B_e(cm^{-1})	11.61	11.63		
C_e(cm^{-1})	7.98	7.96		
Barrier to linearity (cm^{-1})	5132	5373	5071	6200
Excitation energy T_e (cm^{-1})	10193	10159	10475	
b^1B_1	This work		Ref. [1]	Ref. [8]
	$[B_1]^a$	$[B_2]^a$		
R_e(Å)	1.029	1.030	1.034	
α_e(°)	160.92	159.31	164.07	
ν_1	3083	3068		
$2\nu_2$	1404	1401		
ν_3	3304	3289		
Rotational constants				
A_e(cm^{-1})	329.04	279.50		
B_e(cm^{-1})	8.12	8.14		
C_e(cm^{-1})	7.92	7.91		
Barrier to linearity (cm^{-1})	62	98	149	220
Excitation energy T_e (cm^{-1})	15263	15431	15397	

[a] MRCI results calculated with the basis sets $[B_1]$ and $[B_2]$

Fig. 1. One-dimensional cuts of the PEFs for the X^3B_1, a^1A_1 and b^1B_1 states of NH_2^+ along the bending coordinate α

Fig. 2. The pattern of bending levels (up to $K_a = 4$, bent notation) in the electronic ground state X^3B_1 of NH_2^+

Fig. 3. The rotational 000–000 (bent notation) absorption band at 300 K for $J'' = 0$ to 8 in the electronic ground state X^3B_1 of NH_2^+

Fig. 4. The symmetric stretching 100–000 (bent notation) absorption band at 300 K for $J'' = 0$ to 8 in the electronic ground state X^3B_1 of NH_2^+

Fig. 5. The bending 010–000 (bent notation) absorption band at 300 K for $J'' = 0$ to 8 in the electronic ground state X^3B_1 of NH_2^+

Fig. 6. The antisymmetric stretching 001–000 (bent notation) absorption band at 300 K for $J'' = 0$ to 8 in the electronic ground state X^3B_1 of NH_2^+

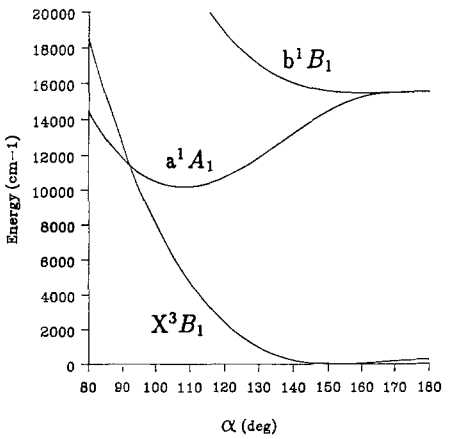
b¹B₁
a¹A₁
X³B₁
Energy (cm−1)
α (deg)

1

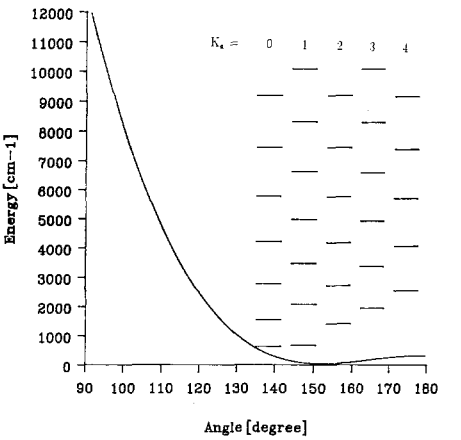
Kₐ = 0 1 2 3 4
Energy [cm−1]
Angle [degree]

2

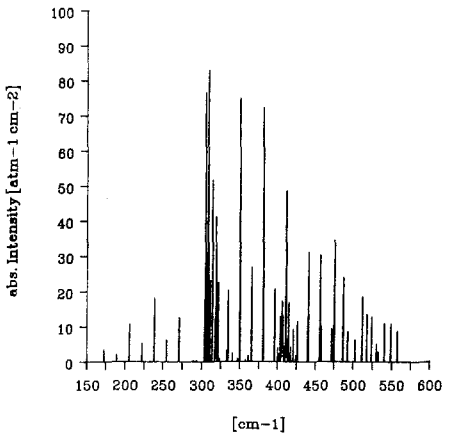
abs. Intensity [atm−1 cm−2]
[cm−1]

3

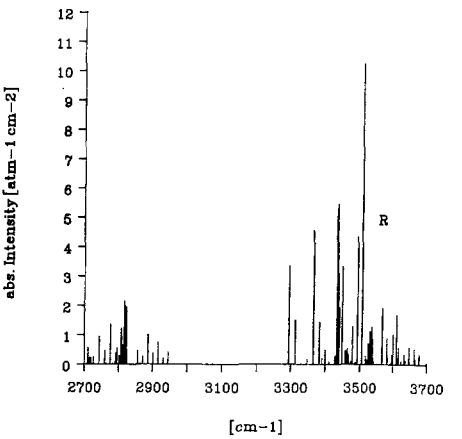
R
abs. Intensity [atm−1 cm−2]
[cm−1]

4

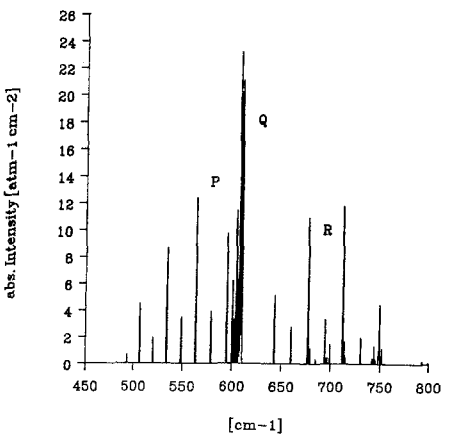
P
Q
R
abs. Intensity [atm−1 cm−2]
[cm−1]

5

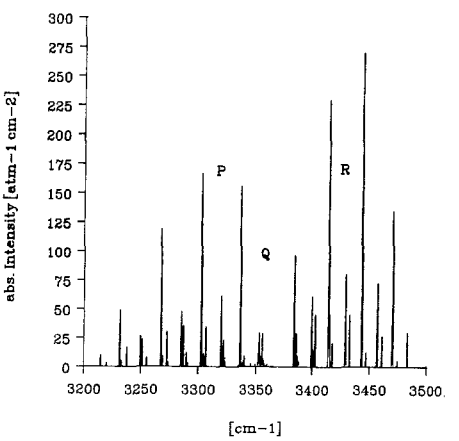
P
Q
R
abs. Intensity [atm−1 cm−2]
[cm−1]

6

Table 9. Some stretching and combination levels ($K = 0$) for the a^1A_1 and b^1B_1 states of NH_2^+ (in cm^{-1})

a^1A_1				b^1B_1			
$(v_1 v_2^{bent} v_3)$		$(v_1 v_2^{bent} v_3)$		$(v_1 v_2^{lin} v_3)$		$(v_1 v_2^{lin} v_3)$	
(1 0 0)	3050	(0 0 1)	3133	(1 0 0)	8771	(0 0 1)	8992
(1 1 0)	4368	(0 1 1)	4446	(1 2 0)	10138	(0 2 1)	10345
(1 2 0)	5621	(0 2 1)	5701	(1 4 0)	11654	(0 4 1)	11838
(2 0 0)	6008	(1 0 1)	6046	(2 0 0)	11770	(1 0 1)	11934
(0 0 2)	6227	(0 3 1)	6893	(0 0 2)	12221	(1 2 1)	13249
(1 3 0)	6807	(1 1 1)	7350	(2 2 0)	13100	(0 6 1)	13447
(2 1 0)	7315	(0 4 1)	8020				
(0 1 2)	7526	(1 2 1)	8594				
(1 4 0)	7933						
(2 2 0)	8557						
(0 2 2)	8770						
(3 0 0)	8849						

anharmonicity, whereas those in the upper state show inverse anharmonicity–like in the electronic ground state.

As expected from the position of the barrier to linearity, the K_a reordering in the bending levels begins in $v_2 = 4$, for which the $K_a = 1$ level for the first time lies lower than the $K_a = 0$ level. In Table 9 additional stretching and combination Σ levels for both electronic states are given.

The only study of the Renner–Teller problem in the NH_2^+ has been performed by Peric, Buenker, and Peyerimhoff [8]. The vibronic bending levels deviate by more than 100 to 150 cm^{-1} from our results, and their energy difference between the lowest levels in the a^1A_1 and the b^1B_1 state by 624 cm^{-1}, due to the different values for the barriers to linearity (cf. Table 7).

Recently, we have investigated the $^2A_1 - {}^2B_1$ Renner–Teller system of the BH_2 radical [21] with almost identical linear spaces in the electronic structure calculations. After an empirical shift of the barrier to linearity in the ground state by -97 cm^{-1}, all experimentally known vibronic energy differences have been reproduced with an accuracy of better than 6 cm^{-1}. Therefore, we expect that the bending Σ levels in the upper $^1B_1$ state of NH_2^+ are calculated to be uniformly too high by about 100 to 150 cm^{-1} relative to the lower lying singlet state. This also implies, however, that the bending levels of the lower singlet state above and close to the calculated barrier to linearity are not very accurate. For this reason we have given only the $K_a = 0$ and 1 levels in Table 8, since the Renner–Teller coupling will be strongly influenced by the position of this barrier. As for BH_2, the three-dimensional PEFs given in Table 1 can be easily modified once experimental data for the bending levels become available. We expect that the calculated stretching frequencies in both singlet states have similar accuracy as in the ground state.

6 Conclusions

In this work high accuracy PEFs for three electronic states of the NH_2^+ ion have been determined by electronic structure calculations. Rotational–vibrational energy levels and wavefunctions have been calculated for the quasi-linear ground state and the Renner–Teller bent/quasi-linear $a^1A_1 - b^1B_1$ system using the

variational method. The few so far experimentally known vibrational transition energies in the electronic ground state have been reproduced with accuracy of about 10 cm^{-1}. More complete experimental information – particularly for the Renner–Teller system – is needed to improve the accuracy of the theoretical potential energy functions of NH_2^+.

Acknowledgements. We would like to thank T. R. Huet, Y. Kabbadj, C. Gabrys, and T. Oka for providing us with experimental results prior to publication and for stimulating discussions, and to H.-J. Werner and P. J. Knowles for the access to the MOLPRO computer code. This work has been supported by the Deutsche Forschungsgemeinschaft, SFB92, Fonds der Chemischen Industrie, PROCOPE grant for German–French collaboration and the EC grant 89200159/OP1. The calculations were carried out on the CRAY YMP, HLRZ, Jülich, Germany.

References

1. Jensen P, Bunker PR, McLean AD (1987) Chem Phys Lett 141:53
2. Peyerimhoff SD, Buenker RJ (1979) Chem Phys 42:167
3. Okumura M, Rehfuss BD, Dinelli BM, Bawendi MG, Oka T (1989) J Chem Phys 90:5918
4. Huet TR, Kabbadj Y, Gabrys C, Oka T (1989) 47th Symp on Molecular Spectroscopy, Columbus, Ohio
5. Dunlavey SJ, Dyke JM, Jonathan N, Morris A (1980) Mol Phys 39:1121
6. Herzberg G (1983) in: Miller TA, Bondybey VE (eds) Molecular ions: Spectroscopy, structure and chemistry. North-Holland
7. Green WH, Chen IC, Bitto H, Guyer DR, Moore CB (1989) J Mol Spectr 138:614
8. Peric M, Buenker RJ, Peyerimhoff SD (1984) Astrophys Lett 24:69
9. DeFrees DJ, McLean AD (1985) J Chem Phys 82:333
10. Green WH, Handy NC, Knowles PJ, Carter S (1991) J Chem Phys 94:118
11. Dunning TH, (1989) J Chem Phys 90:1007
12. Werner HJ, Knowles PJ (1985) J Chem Phys 82:5053
13. Knowles PJ, Werner HJ (1985) Chem Phys Lett 115:259
14. Werner HJ, Knowles PJ (1988) J Chem Phys 89:5803
15. Knowles PJ, Werner HJ (1988) Chem Phys Lett 145:514
16. The CASSCF calculations have been performed with the MOLPRO program suite written by Werner HJ, Knowles PJ, with contributions of Almlöf J, Amos RD, Elbert ST, Meyer W, Reinsch EA, Pitzer RM, Stone AJ, Taylor PR
17. Carter S, Handy NC (1984) Mol Phys 52:1367
18. Carter S, Senekowitsch J, Handy NC, Rosmus P (1988) Mol Phys 65:143
19. Senekowitsch J, Zilch A, Carter S, Werner HJ, Handy NC, Rosmus P (1989) J Chem Phys 90:783
20. Carter S, Handy NC, Rosmus P, Chambaud G (1990) Mol Phys 71:605
21. Brommer M, Rosmus P, Carter S, Handy NC (1992) Mol Phys 77:549